This is a repository copy of *Microstructure development of BiFeO3-PbTiO3 films deposited by pulsed laser deposition on platinum substrates*.

White Rose Research Online URL for this paper:
http://eprints.whiterose.ac.uk/83840/

Version: Accepted Version

**Microstructure development of $BiFeO_3$ – $PbTiO_3$ films deposited by pulsed laser deposition on platinum substrates**

Faye Esat[1], Tim P Comyn[1], Andrew J Bell[1]

[1]Institute for Materials Engineering, School of Process, Environmental and Materials Engineering, University of Leeds, UK, LS2 9JT

e-mail: f.esat@leeds.ac.uk

telephone: +44 (0)113 343 2362

fax: +44 (0)113 343 2549

**Abstract**

BiFeO$_3$-PbTiO$_3$ films around the morphotropic phase boundary were deposited by pulsed laser deposition on polycrystalline Pt/TiO$_x$/SiO$_2$/Si substrates. X-ray analysis confirms that 0.6BiFeO$_3$-0.4PbTiO$_3$ films are (001) tetragonal preferentially orientated due to lattice matching with the underlying substrate. The misfit strain at the substrate – film interface is relieved by a ~19% orientation transformation from (001) to (100) due to the difference in lattice mismatch at the substrate-film interface and thermal expansion coefficients of the substrate and deposited film. 0.7BiFeO$_3$-0.3PbTiO$_3$ films are mixed phase rhombohedral-tetragonal with (001) / (111) preferential orientated due to the lattice match to the (111) and (100) of the underlying platinum as well as being close to the morphotropic phase boundary. Inconsistent structural and electrical properties in reported BiFeO$_3$-PbTiO$_3$ films are explained in terms of film morphology and diffusion of bismuth into platinum. Films below ~220 nm thickness produce short circuits due to a Volmer-Weber growth mechanism which results in physical defects within the films. Films above this critical thickness also produce variable electrical properties due to diffusion of bismuth into the underlying platinum electrode which has been confirmed by energy dispersive X-ray spectroscopy.

**Key Words**

**1. Introduction**

For three decades, ferroelectric thin films have received attention due to their potential applications in memory devices, sensors and signal processing. Memory device technology has mainly focussed on the commercially used lead zirconate titanate (PZT), however the levels of polarization achievable in PZT presents a problem in device scalability where further miniaturization is desired [1]. Over the past decade, materials that offer a higher switchable polarization compared to PZT have been of interest due to their potential use as a scalable high density memory device [2,3].

Thin film multiferroic materials, particularly those of the ferroelectric - ferromagnetic variety, form another research area that has stimulated much scientific and technological interest [4,5]. Identifying materials in which the polarization and magnetization are strongly coupled at room temperature (whereby magnetisation can be strongly influenced by an applied field or the polarization by a magnetic field) would lead to developments in devices for sensing, data storage and signal processing.

The solid solution of $BiFeO_3$ with $PbTiO_3$ known as bismuth ferrite lead titanate ($xBiFeO_3 – ((1-x)PbTiO_3)$, exhibits a morphotropic phase boundary (MPB) between the rhombohedral R3c and tetragonal P4mm phases ($x \approx 0.7$) and is of special interest due to its multiferroic nature and exceptionally high tetragonality (c/a ratio) of approximately 1.17. For these reasons it is a promising material for ferroelectric applications that require high levels of polarization and temperature stability as well as multiferroic properties [6-9]. Switching across this MPB is of interest as it offers the opportunity to exploit three different ferroic order parameters, with the rhombohedral form being

3

antiferromagnetic, the tetragonal form being paramagnetic and both forms ferroelectric, at room temperature. Here there is potential to electrically switch between the paramagnetic and antiferromagnetic forms via a field enforced transition between the tetragonal and rhombohedral phases.

$BiFeO_3$–$PbTiO_3$ thin film research to date has centred around compositions lying close to the MPB, due to the enhanced electrical properties and co-existing antiferromagnetic ordering shown in their bulk counterparts [10,11]. Gupta [12], Sakamoto [13], Singh [14], prepared films around the MPB by chemical solution deposition on $Pt/Ti/SiO_2/Si$ substrates. Although all films were reported to be polycrystalline perovskite, there were inconsistencies in the reported structural space group which were reported as; monoclinic [12], rhombohedral [14] and mixed phase tetragonal-rhombohedral [13]. Although no ferroelectric hysteresis loop was fully saturated, the remnant polarization varied in the reports; $2Pr = 50\mu C/cm^2$ (measured at -190°C) [13], $36\mu C/cm^2$ [12] and $1\mu C/cm^2$ [14]. Using the same deposition technique Lui [15] reported multiferroic properties in $BiFeO_3$–$PbTiO_3$ films on $LaNiO_3/SiO_2/Si$ substrates. For films with x = 0.2 and 0.3, $2Pr = 1.7\mu C/cm^2$ and $2.05\mu C/cm^2$ with ferromagnetic properties of $M_s$ 26.4emu $cm^{-3}$ and 21.98emu $cm^{-3}$.

Pulsed laser deposited $BiFeO_3$–$PbTiO_3$ films on $Pt/Ti/SiO_2/Si$ substrates generally report improved electrical properties to those produced by chemical solution deposition, however inconstancies still remain. Yu [16] prepared polycrystalline hetrostructure $ZnO/BiFeO_3$–$PbTiO_3$ composite films and $BiFeO_3$–$PbTiO_3$ film on $Pt/Ti/SiO_2/Si$ substrates by pulsed laser deposition (PLD). Although polarisation – electric field (P-E) hysteresis loops were detectable at

room temperature they were not fully saturated with a remnant polarization of $2P_r$ of 32 µC/cm$^2$ (ZnO/BiFeO$_3$ – PbTiO$_3$) and 6µC/cm$^2$ (BiFeO$_3$ – PbTiO$_3$). Khan reported significant improvements in films produced by PLD with saturated P-E hysteresis loops for the 0.6BiFeO$_3$ – 0.4PbTiO$_3$ compositions on Pt/Ti/SiO$_2$/Si substrates, exhibiting switchable polarizations up to 80 µCcm$^{-2}$ in weakly textured films around the MPB [17] and upto 60 µCcm$^{-2}$ in 0.2BiFeO$_3$-0.8PbTiO$_3$ films when measured at -10˚C [18]. More recently Chen reported films deposited by PLD of 0.72Bi(Fe$_{1-x}$Ti$_x$)O$_3$-0.28PbTiO$_3$ (x = 0 and 0.02) on Pt/TiO$_x$/SiO$_2$/Si substrates. Although P-E ferroelectric hysteresis loops were not completely saturated a large remnant polarization of 80 µCcm$^{-2}$ was obtained in the doped films at room temperature [19,20].

Although the pulsed laser deposited films show a significant improvement in the electrical properties of undoped xBiFeO$_3$ - (1-x)PbTiO$_3$ thin films compared to other processing techniques, reproducibility proved to be an issue [17]. To achieve the fully saturated P-E hysteresis loops, hundreds of attempts were made using different preparation conditions and electrodes and subsequent work has shown that these properties are somewhat difficult to reproduce. This is also consistent with the wide variety of data reported by various authors. For these reasons a detailed study has been carried out in an attempt to understand the origins of these inconsistencies.

This paper reports on PLD produced xBiFeO$_3$ – (1-x)PbTiO$_3$ x = 0.7 and 0.6 thin films close to the reported MPB (x = 0.7) onto Pt/TiO$_x$/SiO$_2$/Si substrates, which allows comparisons to be made against the existing literature. It is widely reported that the structural properties of thin films are thickness

dependent, however BiFeO$_3$ -PbTiO$_3$ thin films have not received as much interest as their bulk counterpart and little work has been published on the effect of film thickness on structural properties. Therefore to gain a more in depth understanding of the origin of inconsistencies in reported results and irreproducibility of the films, a detailed analysis has been carried on the effect of film thickness and film composition.

## 2. Experimental Procedure

### 2.1. Sample Preparation

xBiFeO$_3$ – (1-x)PbTiO$_3$ compositions with x = 0.7 and 0.6 were prepared by mixing stoichiometric ratios of PbO, TiO$_2$, Bi$_2$O$_3$ and Fe$_2$O$_3$ powders (>99% purity, Sigma Aldrich, Germany) ball milled for 24 hours and attrition milled for 30 minutes. The milled powders were dried and sieved through a 300 micron mesh. The powders were then calcined at 800 °C for 2 hours, attrition milled and sieved before being isostatically pressed at 400 MPa to achieve a high green density in the PLD targets. Finally the targets were sintered at 1000 °C for 30 minutes.

A Tui Thin Film Star 248nm KrF laser system (TuiLaser AG, Munich, Germany) incorporated into a Surface PLD Workstation (Surface AG, Hucklehoven, Germany) was used to deposit material onto the polycrystalline platinum substrates. All films were deposited on Pt 200nm/TiOx 50nm/SiO$_2$ 500nm/Si substrates (PIKEM, UK) which were ultrasonically cleaned in acetone and isopropanol for 5 minutes each before deposition. They were then rinsed in deionized water and dried.

All films were deposited at a frequency of 5 Hz, substrate temperature of 565 °C with an oxygen partial pressure of 75 mTorr and a post deposition anneal temperature of 600 °C. Details for optimum processing conditions of $BiFeO_3$-$PbTiO_3$ thin films on $Pt/TiO_x/SiO_2/Si$ can be found elsewhere [17].

## 2.2. Sample Characterisation

The film thickness was varied from 110 nm to 1360 nm by controlling the number of laser pulses and was confirmed by scanning electron microscopy (SEM) cross sectional analysis. X-ray diffraction (XRD: X'Pert PRO MPD, PANalytical) was performed using Cu $K_\alpha$ radiation to characterise the crystallographic structure and phase identification of the deposited films. The Bragg – Brentano configuration was used to produce scans with a 2θ range from 15 - 60°, a step size of 0.033° and a scan speed of 0.05°$^{-1}$. Atomic force microscopy (AFM: Agilent 5420 series) was performed to image surface topography from which the root mean squared roughness was calculated and transmission electron microscopy (TEM: Phillips CM200) with energy dispersive x-ray (EDX: Oxford Instruments) was performed to analysis the composition across the film cross sections.

## 3. Results

### 3.1. 0.6BiFeO$_3$ – 0.4PbTiO$_3$ Film Structure

Figure 1 shows x-ray diffraction patterns of 0.6BiFeO$_3$ – 0.4PbTiO$_3$ thin films. As compared with the bulk ceramic targets from which the films were processed, the enhanced intensity of the {100} suggests the films have a preferred texture. In addition, the (101), which is the most intense peak in the bulk ceramic target,

is absent from the films until the films have started to relax at increased thicknesses (1360 nm). At increased thicknesses the films appear to develop a more 'bulk-like' structure with the enhanced intensity of the (111) and (101), however the films remain {100} preferentially orientated compared to the bulk ceramic target. The presence of texture at reduced thicknesses indicates that the films are influenced by the orientation of the underlying substrate rather than adapting the bulk relaxed form. Although the films are not a single preferred orientation, this is still referred to as preferential orientation.

The degree of orientation can be defined by a semiquantatative method using the lotgering factor, $f$, which was calculated to be 0.73 for the {100} orientation for the film.

$$f = (p - p_o) / (1 - p_o) \qquad (1)$$

where $P$ and $P_0$ are equal to $I(mnp)/\sum(hkl)$ for an oriented and unoriented sample along the [$mnp$], respectively.

In bulk materials the diffraction peaks from the (001) and (100) tetragonal are from the a- and c-axis of the unit cell, therefore knowing the (100) d-spacing the (001) d-spacing can be calculated. However, unlike bulk materials, these assumptions cannot be made in thin films because the diffraction peak from the (001) and the (100) may not be from the same size unit cell. Therefore to accurately index the individual peaks and calculate the d-spacings, peak profile fittings have been carried out using WinPlotR which is part of the Full Prof Suite Software package.

Figure 2 shows the {100} peak profile fittings for the various film thicknesses. Three peaks have been identified P1, P2 and P3. From the peak profile fits, the corresponding d-spacings and peak heights for the various film thicknesses are shown in Table 1.

Table 1. The measured d-spacings of the three peaks identified in the peak profile fittings for $0.6BiFeO_3 – 0.4PbTiO_3$ films using WinPlotR with corresponding peak heights.

| Film Thickness (nm) | d-spacing P1 (Å) | d-spacing P2 (Å) | d-spacing P3 (Å) | Peak Height P1 | Peak Height P2 | Peak Height P3 |
|---|---|---|---|---|---|---|
| 110 | 4.50 | 4.14 | 3.90 | 0.13 | 0.8 | 0.07 |
| 150 | 4.54 | 4.15 | 3.92 | 0.16 | 0.78 | 0.06 |
| 460 | 4.55 | 4.13 | 4.10 | 0.11 | 0.79 | 0.10 |
| 620 | 4.53 | 4.13 | 4.00 | 0.12 | 0.79 | 0.09 |
| 1360 | 4.53 | 4.13 | 4.00 | 0.10 | 0.72 | 0.18 |

To determine the preferential orientation direction and misfit strain on the deposited unit cells, the known lattice parameters of bulk $0.6BiFeO_3 – 0.4PbTiO_3$ at room temperature and 565 °C (the deposition temperature) must both be considered to understand the possible orientation development and lattice matching to the substrate. The interatomic spacings describe closely matching lattice parameters between platinum (100) (a = 3.94 Å) and the $0.6BiFeO_3 – 0.4PbTiO_3$ (001) (a = 3.96 Å) and (100) (a = 3.96 Å, c = 4.06 Å) at the deposition temperature [8,21]. In addition the (001) plane is square which may also increase the likelihood of hetroepitaxial match to the cubic structure of the platinum substrate. Although (001) preferential orientation seems likely, misfit strain will still be present at the substrate-film interface which may be

compensated for with (100) orientated material, as this is a close lattice match to the underlying platinum.

As the film cools from the deposition temperature to room temperature, the tetragonality of bulk $0.6BiFeO_3 – 0.4PbTiO_3$ increases with an increase in the c-axis and a decrease in the a-axis, therefore increasing the in-plane misfit strain between the platinum (100) (a = 3.92 Å) and the $0.6BiFeO_3 – 0.4PbTiO_3$ (001) (a = 3.84 Å) and (100) (a = 3.84 Å, c = 4.44 Å) [8,21]. Although it seems likely that the film develops a (001) and (100) preferential orientation at the deposition temperature this change in tetragonality increases the in-plane misfit strain in the (100) much more than the square (001) which the system will attempt to relieve. If any of the deposited film was orientated in the [100] direction when held at the deposition temperature, it is likely that the (100) orientated planes will transform to (001) when cooled to room temperature due to the more closely matched in-plane lattice parameters between the platinum (100) and the cubic interatomic spacing of the $0.6BiFeO_3 – 0.4PbTiO_3$ (001). As P2 is the most intense peak (Figure 1) throughout the film thickness range and is closely matched to the d-spacing seen for the (001) in the bulk counterpart P2 has been indexed as the (001) for the $0.6BiFeO_3 - 0.4PbTiO_3$ films.

The d-spacing of P3 is similar to the d-spacing of the (100) in the bulk $0.6BiFeO_3 - 0.4PbTiO_3$ and when the difference in d-spacing between P2 and P3 is compared to the difference seen in its bulk counterpart (100) and (001), it is likely that P3 is the (100) of the deposited film (to retain a similar unit cell volume). In Table 1 the relative peak height of P2 and P3 describe a highly (001) preferred orientation at reduced film thicknesses. With increasing

thickness, the relative intensity of the (001) (P2) reduces and an increase in relative intensity of the (100) (P3) is observed. This may be attributed to relaxation of the films preferred orientation with increasing distance from the substrate. However, throughout the thickness range the $0.6BiFeO_3 - 0.4PbTiO_3$ films remain (001) preferentially orientated.

Although the (001) is a close match to the structure of the underlying substrate the misfit between the platinum and $0.6BiFeO_3 - 0.4PbTiO_3$ unit cell parameters still remains. The strain that will arise from this appears to have been compensated for by the presence of the closely matching (100) orientation that increase in intensity with increasing thickness. To calculate the fraction of unit cells which would need to transform to the (100) orientation in order to compensate for the misfit strain present in (001) orientated films, the thermal expansion coefficient of the underlying silicon needs to be considered.

Assuming hetroepitaxial matching when at the deposition temperature, a length ($L$) of unit cells in the deposited film, with an a-axis ($a$) lattice parameter, the number of unit cells ($n$) is approximately equal to:

$$n = L/a \qquad\qquad (2)$$

As the film is cooled to room temperature the silicon substrate contracts to the new length $L'$

$$L' = L\,(1 - \alpha\Delta T) \qquad\qquad (3)$$

where $\Delta T$ is the change in temperature and $\alpha$ is the approximate thermal expansion coefficient of silicon ($2.6 \times 10^{-6}\ °C^{-1}$).

Some of the $BiFeO_3$ – $PbTiO_3$ lattice parameters change to compensate for the thermal expansion mismatch. *m* unit cells have the c-axis in-plane and the remaining unit cells (*n-m*) have the a-axis in the plane.

$$L' = (n - m)\, a' + mc' \qquad (4)$$

Where *a'* and *c'* are the a-axis and c-axis lattice parameters at room temperature.

From equation (2), (3) and (4), the fraction of unit cells which need to be (100) orientated to relieve the mis-fit strain in a (001) hetroepitaxial film is therefore

$$m/n = (a(1 - \alpha\Delta T) - a') / (c' - a') \qquad (5)$$

The lattice parameters of the $0.6BiFeO_3$ – $0.4PbTiO_3$ film at the deposition temperature and room temperature can then be substituted into the above equation.

The lattice parameters have been calculated for the temperatures of interest by graphically extrapolating existing data points for platinum, $0.6BiFeO_3$ – $0.4PbTiO_3$ and $0.7BiFeO_3$ – $0.3PbTiO_3$ from existing literature [21,8].

*a = 3.96, c = 4.06, a' = 3.838, c' = 4.438*

*therefore m/n = 0.19*

Approximately 19% of the unit cells need to transform from (001) orientated to (100) orientated to relieve the strain imparted at the substrate – film interface with decreasing temperature from the deposition temperature. Which agrees with the relative height intensities of the two corresponding peaks in Table 1.

## 3.2. $0.7BiFeO_3$ – $0.3PbTiO_3$ Film Structure

Figure 3. shows x-ray diffraction patterns of $0.7BiFeO_3$ - $0.3PbTiO_3$ films of different thicknesses on $Pt/TiO_x/SiO_2/Si$ substrates. Again the d-spacings and peak heights for various film thicknesses for the {100} preferential orientation have been determined from peak profile fittings using WinPlotR (Figure 4) and can be seen in Table 2.

Although it appears the films are influenced by the substrate structure, the change in $xBiFeO_3$ – $(1-x)PbTiO_3$ composition produces a film that less readily grows hetroepitaxial to one particular plane of the underlying platinum substrate.

Table 2. The measured d-spacings of the four peaks identified in the peak profile fittings for $0.7BiFeO_3$ – $0.3PbTiO_3$ films using WinPlotR with corresponding peak heights.

| Film Thickness (nm) | d-spacing P1 (Å) | d-spacing P2 (Å) | d-spacing P3 (Å) | d-spacing P4 (Å) | Peak Height P1 | Peak Height P2 | Peak Height P3 | Peak Height P4 |
|---|---|---|---|---|---|---|---|---|
| 110 | 4.55 | 4.13 | 4.03 | 3.94 | 0.05 | 0.32 | 0.27 | 0.36 |
| 150 | 4.59 | 4.14 | 4.03 | 3.93 | 0.05 | 0.21 | 0.23 | 0.50 |
| 290 | 4.53 | 4.14 | 4.02 | 3.93 | 0.07 | 0.26 | 0.34 | 0.33 |
| 460 | 4.53 | 4.11 | 4.02 | 3.93 | 0.06 | 0.22 | 0.43 | 0.28 |
| 620 | 4.51 | 4.10 | 4.00 | 3.90 | 0.06 | 0.27 | 0.36 | 0.31 |
| 1120 | 4.51 | 4.12 | 4.02 | 3.93 | 0.05 | 0.23 | 0.34 | 0.38 |
| 1360 | 4.53 | 4.13 | 4.02 | 3.94 | 0.06 | 0.22 | 0.48 | 0.24 |

Analysis of the peak profile fittings shows P1 has the same d-spacings as the peak associated with the secondary phase in the $0.6BiFeO_3$ – $0.4PbTiO_3$ films

therefore it is likely that P1 is associated with a secondary phase from possible substrate film interactions. The d-spacings of P2 and P4 are very similar to those indexed as the (001) and (100) in the $0.6BiFeO_3 – 0.4PbTiO_3$ films, with the 110nm films producing a difference in d-spacing of 0.007 Å for P2 and 0.09 Å for P4. Therefore P2 has been indexed as $(001)_{tetragonal}$ and P4 as $(100)_{tetragonal}$.

P3 is situated between the (001) and (100) tetragonal in the x-ray trace and has a d-spacing of 4.03 Å. This d-spacing is very close to the rhombohedral (100) d-spacing seen in its bulk counterpart. As the $0.7BiFeO_3 – 0.3PbTiO_3$ composition is located on the MPB between the tetragonal P4mm and rhombohedral R3c phase, it is not unexpected that the tetragonal and rhombohedral phases to co-exist in the same film to produce a mixed phase film. It therefore seems likely that P3 is associated with the (100) of the rhombohedral phase. Further evidence of this is obtained from analysis of the peak heights (Table 2) with P3 increasing in intensity with increasing thickness to become the most dominant peak as the film is able to relax from the constraints of the substrate.

## 3. Growth Mechanism

As can be seen in Figure 5, below 290 nm, 40,000 pulsed laser shots, there is a linear increase in thickness with respect to the number of pulses emitted from the laser. Above 290 nm the linear response is still observed however, there is a change in gradient at 290 nm film thickness.

To investigate this in further detail the surface profiles of $0.7BiFeO_3 - 0.3PbTiO_3$ and $0.6BiFeO_3 - 0.4PbTiO_3$ films on $Pt/TiO_x/SiO_2/Si$ substrates were analysed

14

by atomic force microscopy (AFM) for various film thicknesses, Figure 6. When comparing the surface profile and morphology of the 110 nm film to the 290 nm film, the peak-to-trough distance decreases with increasing thickness. It can also be seen that the grain size increases with increasing thickness. This suggests that any material deposited after the film has exceeded 110 nm, nucleates in the holes between the grains already deposited, resulting in the reduced peak-to-trough distance. The already existing grains then grow at the expense of the smaller grains resulting in an increased grain size. As a result the average peak-to-trough is reduced from ~70 nm (for 110 nm films) to ~ 30 nm (for 150 nm films), producing a more uniform thickness. The AFM analysis also confirms a mono-modal grain height distribution at 110 nm and a bi-modal grain height distribution at 150 nm. As the thickness is increased to 290 nm the average peak-to-trough remains relatively low at ~ 50 nm with a mono-modal height distribution. This suggests that the Volmer-Weber [22] growth mechanism is occurring at the lower thicknesses, resulting in island formation. The Volmer-Weber island mechanism will continue to occur as the thickness of the film is increased due to the topography that is already present from the underlying deposited film. This is evident as the films approach a thickness between ~1120 - 1360 nm where the average peak-to-trough dramatically increases and develops a bi-modal distribution. This suggests that the thicker $0.7BiFeO_3$ - $0.3PbTiO_3$ films on $Pt/TiO_x/SiO_2/Si$ begin to grow in a columnar structure z-direction when in a more relaxed state. This can be seen by the increase in intensity of the (111) c-axis with increasing thickness (Figure 3).

When comparing the surface profile and morphology for the $0.6BiFeO_3$ -

15

0.4PbTiO$_3$ films (Figure 7) of the 110 nm film to the 290 nm film, the peak-to-trough distance decreases with increasing thickness even more than that seen in the 0.7BiFeO$_3$ - 0.3PbTiO$_3$ films (Figure 6). Unlike the 0.7BiFeO$_3$ - 0.3PbTiO$_3$ films, it is only when the 290 nm film thickness is obtained that the average peak-to-trough is reduced and a mono-modal distribution is observed. At ~ 290 nm the average grain size also increases, suggesting that any material present before ~ 290 nm nucleates in the holes between the grains already deposited and grows at the expense of the smaller grains resulting in an increased grain size. AFM (Figure 7) shows the 0.6BiFeO$_3$ - 0.4PbTiO$_3$ films on Pt/TiO$_x$/SiO$_2$/Si grow into a plate-like structure suggesting the {100} plane sits parallel to the (100) plane of the platinum substrate resulting in the {100} preferred orientation throughout the thickness range.

At ~290 nm both the 0.7BiFeO$_3$ - 0.3PbTiO$_3$ and 0.6BiFeO$_3$ - 0.4PbTiO$_3$ films go from appearing conductive (7 Ω) to resistive (> 10 MΩ). Based on the AFM analysis it is probable that the surface morphology of the films below ~ 290 nm results in electrical short circuits through the film. Once the thickness is increased above ~ 290 nm, the films appear resistive suggesting that any holes within the films structure are no longer present as the Volmer-Weber growth mode fills the holes therefore the platinum bottom electrode is no longer exposed.

From these results it appears the conductivity at reduced thicknesses is a direct result of surface morphology of the BiFeO$_3$ – PbTiO$_3$ deposited films. By increasing the thickness beyond 290 nm the films are no longer conductive due to the absence of physical defects within the structure of the deposited film.

Theoretically at a film thickness > 290 nm the films should be able to sustain a P-E loop once the platinum bottom electrode is no longer exposed, however despite the films being of a thickness that completely covers the exposed Pt bottom electrode, they were still unable to achieve fully saturated ferroelectric P-E loops. To investigate this in greater depth, additional microstructural analysis was performed (Figure 8).

On analysis of the films using TEM EXD analysis it appears that all the films suffer significant diffusion of bismuth into the underlying platinum at the substrate – film interface. EDX analysis (Figure 8) shows an increase in bismuth concentration (relative to lead, titanium and iron) in the platinum bottom electrode layer and resulting iron-rich regions in the deposited film. The bismuth and lead move through the entire platinum bottom electrode and sit just above the titanium adhesion layer. It appears that the bismuth moves through the platinum forming porous channels rather than a uniform rate of degradation on the top surface of the electrode. The diffusion of bismuth results in a porous platinum layer that is unable to act as a bottom electrode. It is only when the critical thickness is exceeded that the films no longer suffer severe bismuth and lead loss throughout the entire film surface. Although the XRD data in Figure 1 and 2 provide evidence for the presence of a secondary phase, at 290 nm the relative intensity of the corresponding peak has reduced compared to that seen the thinner samples and therefore indicates that the secondary phase may be confined to certain areas rather than throughout the entire film. The damage to the platinum bottom electrode prevents it acting as a bottom electrode and the integrity of any measurement is compromised by the reaction with Bi and

therefore a P-E hysteresis loop cannot be achieved even at increased thicknesses.

## 4. Conclusion

The $0.6BiFeO_3 – 0.4PbTiO_3$ films were all tetragonal with (001) preferential orientation due to the close matching of lattice parameters with the underlying substrate at room temperature. The mismatch strain that partially derives from the varying thermal expansion coefficients of the deposited film and substrate is compensated for by the development of (100) orientated grains. With increasing thickness the contribution from the (100) increases although the (001) remains the preferred orientation.

The $0.7BiFeO_3 – 0.3PbTiO_3$ films are not orientated in one direction, however the structure is still substrate influenced, displaying tetragonal {100} and (111) preferential orientation. The identification of an extra peak in the x-ray traces suggests the films are tetragonal-rhombohedral mixed phase. The rhombohedral phase (100) becomes the most dominant phase at increased thickness as the film is unable to accommodate the strain at the substrate film interface.

At ~290nm both the $0.7BiFeO_3 - 0.3PbTiO_3$ and $0.6BiFeO_3 - 0.4PbTiO_3$ films go from being conductive (7 $\Omega$) to resistive (~ 10 M$\Omega$). This is due to the topography of the films structure whereby the peak-to-trough distance of some grains can be equal to the thickness of the film. The $0.7BiFeO_3 - 0.3PbTiO_3$ films develop a columnar polycrystalline structure and the $0.6BiFeO_3 - 0.4PbTiO_3$ films develop a plate like polycrystalline structure with large peak-to-

trough distances. This structure leaves the platinum bottom electrode exposed and results in a short circuit, which results in the film appearing conductive. Once the film thickness exceeds 290 nm additional ablated material from the laser plume fills any remaining holes between the grains therefore covering the platinum bottom electrode. However the damage to the platinum bottom electrode by diffusion of bismuth into platinum and resulting chemical inhomogeneities, prevents the platinum acting as a bottom electrode and therefore a P-E loop cannot be achieved even at increased film thicknesses. Therefore despite platinized silicon being a default substrate for device development it is not suitable for this system.

## 5. Acknowledgments

## 6. References

[1] Fujisaki Y. Jpn J Appl Phys 2010;49:100001.

[2] deAraujo CAP, Cuchiaro JD, Mcmillan LD, Scott MC, Scott JF. Nature 1995;374:627.

[3] Wang J, Zheng H, Ma Z, Prasertchoung S, Wuttig M, Droopad R, Yu J, Eisenbeiser K, Ramesh R. Appl Phys Lett 2004;85:2574.

[4] Fiebig M. J Phys D Appl Phys 2005;38:R123.

[5] Hill NA. J Phys Chem B 2000;104:6694.

[6] Zhu WM, Guo HY, Ye ZG. Phys Rev B 2008;78:014401.

[7] Bhattacharjee S, Tripathi S, Pandey D. Appl Phys Lett 2007;91:042903.

[8] Sunder VVSSS, Halliyal A, Umarji AM. J Mater Res 1995;**10:**1301.

[9] Fedulov SA, Ladyzhinskii PB, Pyatgorskaya IL, Venevtsev YN. Sov Phys Solid State 1964;**6:**375.

[10] Stevenson T, Comyn TP, Daoud-Aladine A, Bell AJ. J Magn Magn Mater 2010;**322:**L64.

[11] Comyn TP, Stevenson T, Al-Jawad M, Andre G, Bell AJ, Cywinski R. J Magn Magn Mater 2011;**323:**2533.

[12] Gupta S, Garg A, Agrawal DC, Bhattacharjee S, Pandey D. J Appl Phys 2009;**105:**014101.

[13] Sakamoto W, Yamazaki H, Iwata A, Shimura T, Yogo T. Jpn J Appl Phys 1 2006;**45:**7315.

[14] Singh VR, Kar S, Garg A. Indian J Eng Mater Sci 2008;**15:**104.

[15] Liu HR, Liu ZL, Liu Q, Yao KL. J Phys D Appl Phys 2006;**39:**1022.

[16] Yu SW, Chen R, Zhang GJ, Cheng JR, Meng ZY. Appl Phys Lett 2006;**89:**212906.

[17] Khan MA, Comyn TP, Bell AJ. Appl Phys Lett 2007;**91:**032901.

[18] Khan MA, Comyn TP, Bell AJ. Acta Mater 2008;**56:**2110.

[19] Chen L, Ren W, Zhu W, Ye ZG, Shi P, Chen X, Wu X, Yao X. Thin Solid Films 2010;**518:**1637.

[20] Chen L, Ren W, Zhu W, Ye ZG, Shi P, Chen X, Wu X, Yao X. Ferroelectrics 2011;**410:**42.

[21] Arblaster JW. Platin Met Rev 1997;**41:**12.

[22] Floro JA, Hearne SJ, Hunter JA, Kotula P, Chason E, Seel SC, Thompson CV. J Appl Phys 2001;**89:**4886.

## 7. List of Figures
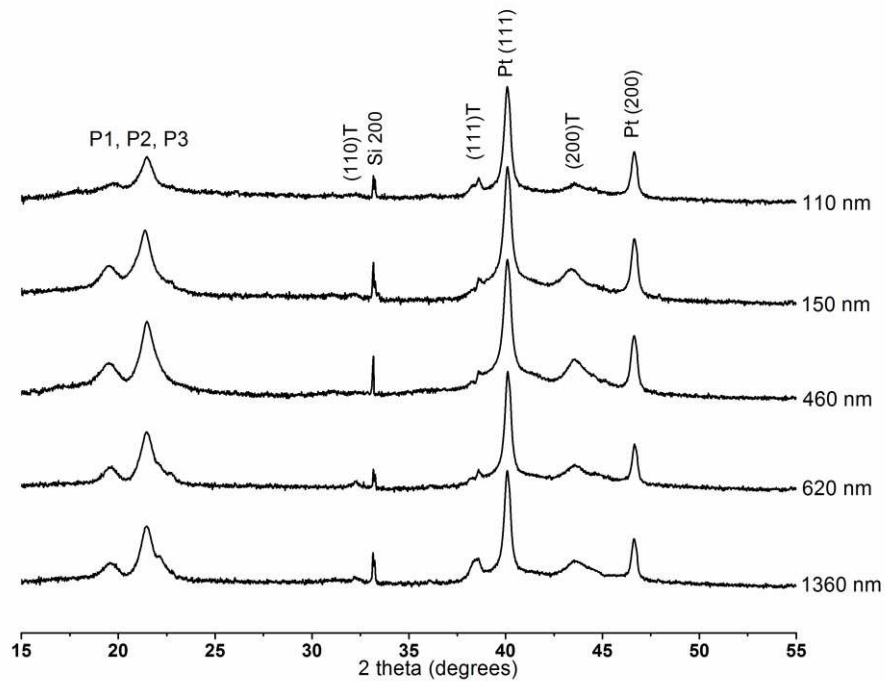


Figure. 1. XRD for $0.6BiFeO_3$ - $0.4PbTiO_3$ films on $Pt/TiO_x/SiO_2/Si$ substrates.
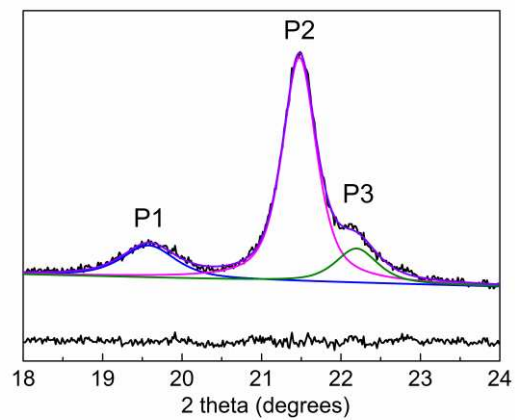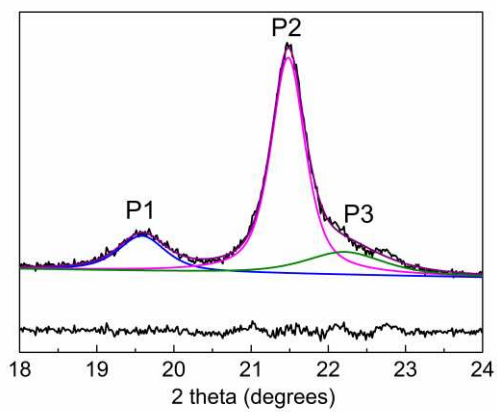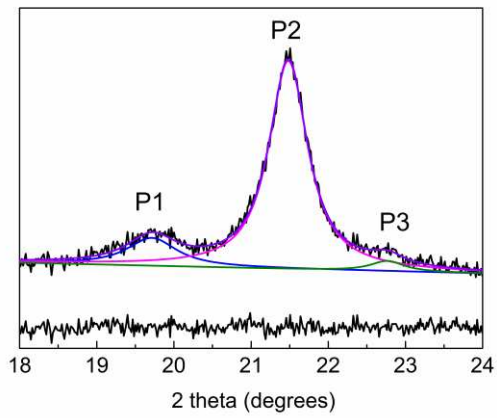
Figure. 2. X-ray {100} peak profile fitting for 0.6BiFeO$_3$ - 0.4PbTiO$_3$ films of thickness a) 110 nm, b) 620 nm, c) 1360 nm. P1, P2 and P3 are the three peaks identified.
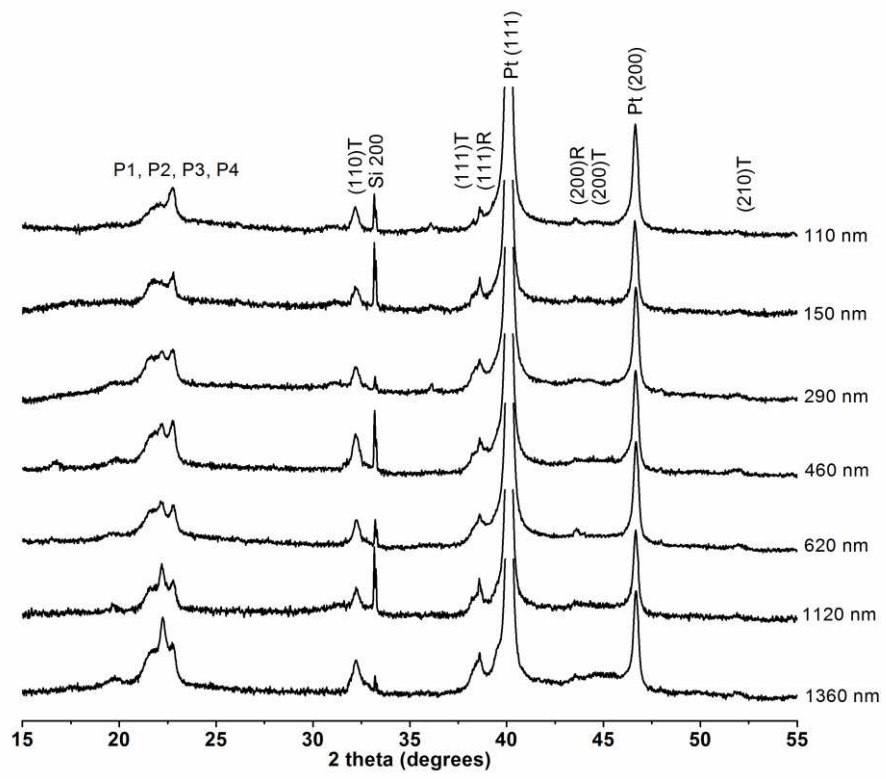
Figure. 3. XRD for $0.7BiFeO_3$ - $0.3PbTiO_3$ films on $Pt/TiO_x/SiO_2/Si$ substrates.
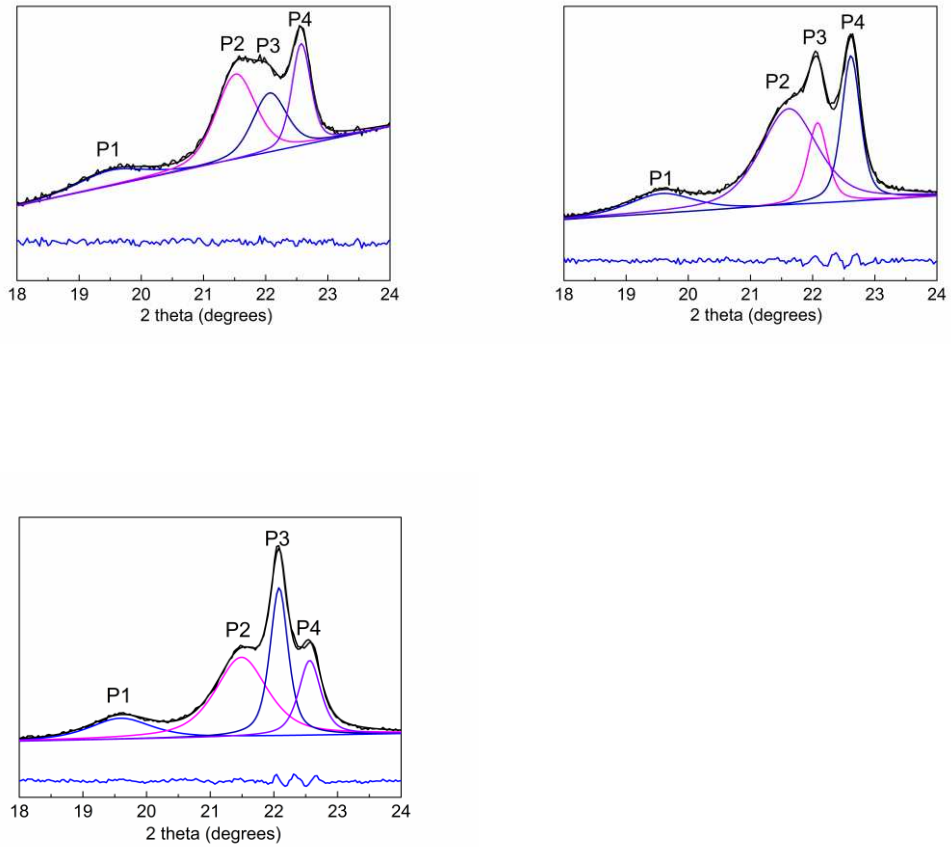
Figure. 4. X-ray {100} peak profile fitting for $0.7BiFeO_3$ - $0.3PbTiO_3$ films of thickness a) 110 nm, b) 460 nm, c) 1360 nm. P1, P2, P3 and P4 are the three peaks identified.
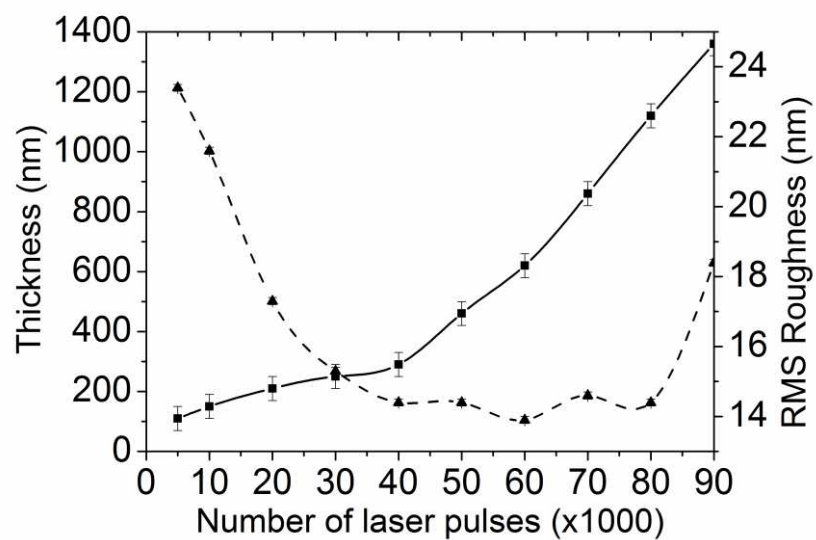
Figure. 5. Thickness (■) and RMS roughness (▲) as a function of the number of

laser pulses for $0.7BiFeO_3$ - $0.3PbTiO_3$ films on $Pt/TiO_x/SiO_2/Si$ substrates.
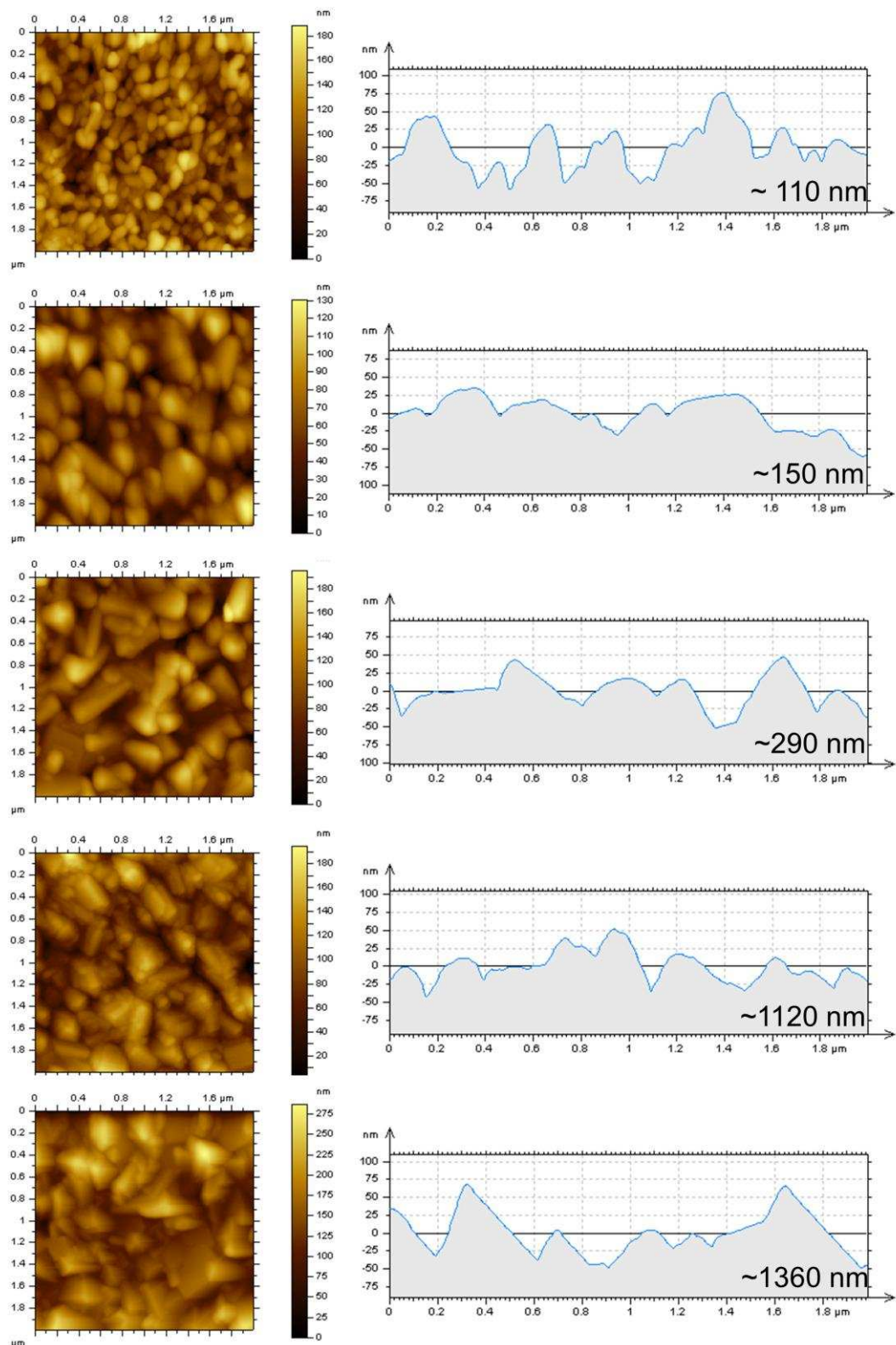
Figure 6. A 2D AFM 2 x 2 μm image of the surface of $0.7BiFeO_3$ - $0.3PbTiO_3$ films, of different thicknesses, on polycrystalline $Pt/TiO_x/SiO_2/Si$ substrates and a profile plot of the morphology.
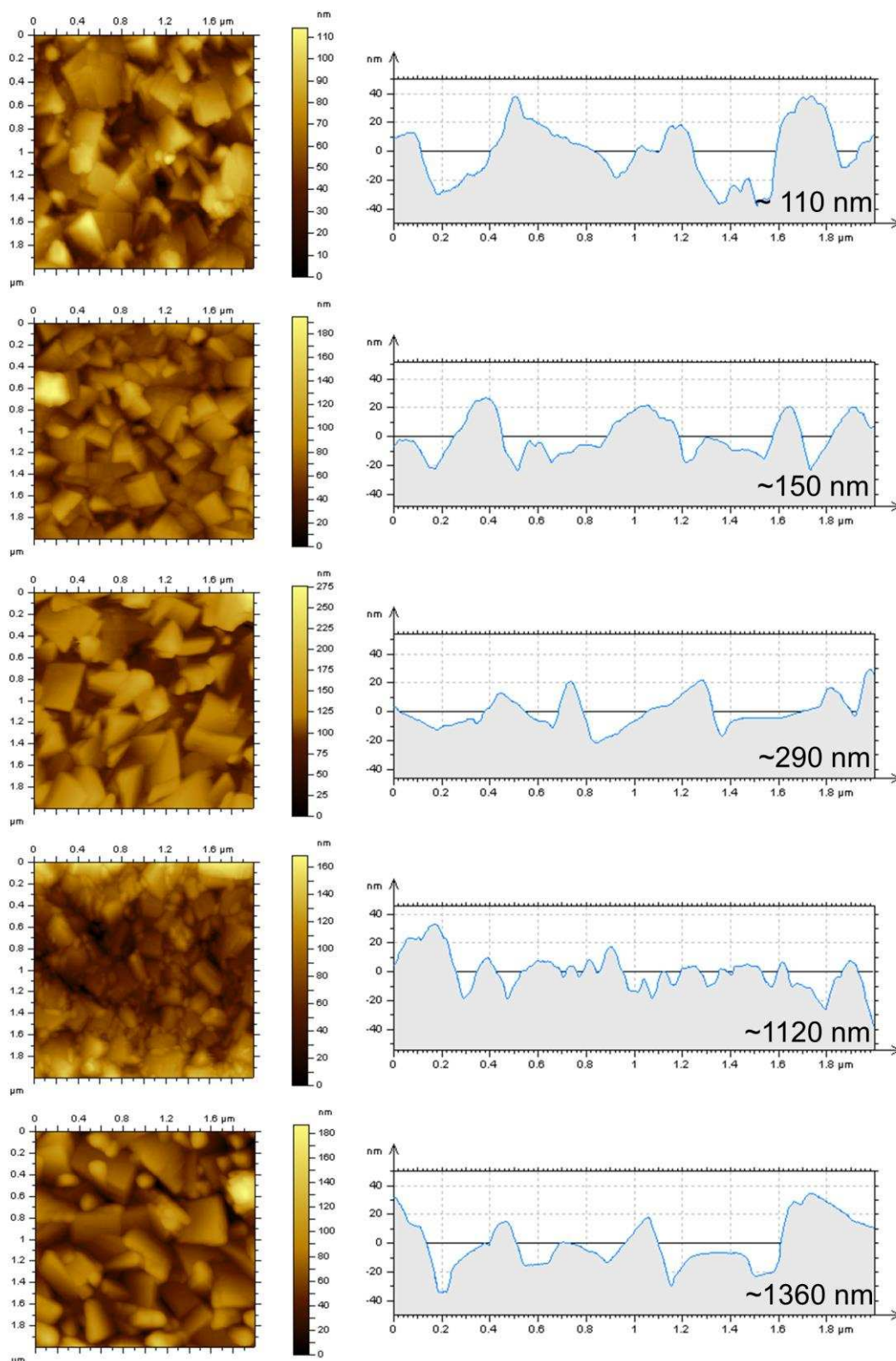
Figure 7. A 2D AFM 2 x 2 μm image of the surface of $0.6BiFeO_3$ - $0.4PbTiO_3$

films, of different thicknesses, on polycrystalline $Pt/TiO_x/SiO_2/Si$ substrates and

a profile plot of the morphology.
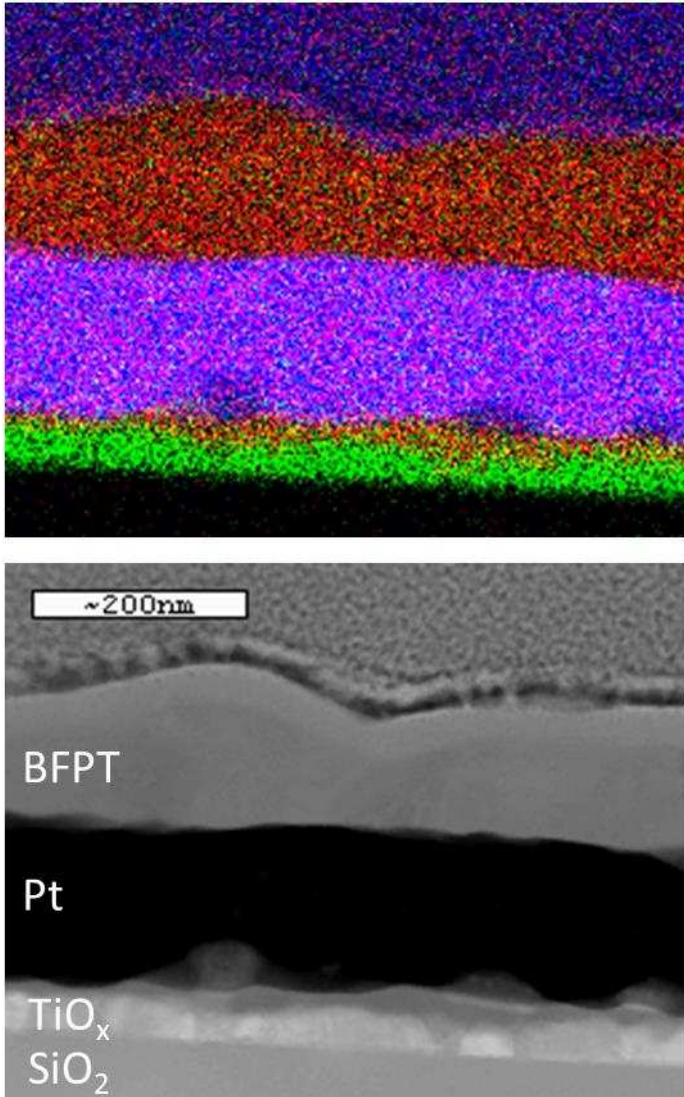
Figure 8. TEM EDX analysis ~ 150 nm thick $0.7BiFeO_3$ - $0.3PbTiO_3$ film (*BFPT). Bottom: TEM dark field image. Top: EDX elemental map of the film (Red = Bi, Yellow = Pb, Blue = Fe, Green = Ti, Purple = Pt.

**8. List of Tables**

Table 1. The measured d-spacings of the three peaks identified in the peak profile fittings for $0.6BiFeO_3$ – $0.4PbTiO_3$ films using WinPlotR with corresponding peak heights.

Table 2. The measured d-spacings of the four peaks identified in the peak profile fittings for $0.7BiFeO_3 - 0.3PbTiO_3$ films using WinPlotR with corresponding peak heights.